DOI: 10.1021/ic9014459

Inorganic Chemistry
Article

Synthesis, Structure, and Electrochemistry of the Dicluster Molecular Pincer $[Pt_3(\mu\text{-}PBu^t_2)_3(CO)_2]_2(\mu\text{-}1',1'''\text{-diethynylbiferrocene})$

Alberto Albinati,[‡] Federica Balzano,[†] Fabrizia Fabrizi de Biani,[§] Piero Leoni,*[,†] Gabriele Manca,[†] Lorella Marchetti,[†] Silvia Rizzato,[‡] Gloria Uccello Barretta,[†] and Piero Zanello[§]

[†]*Dipartimento di Chimica e Chimica Industriale, Università di Pisa, Via Risorgimento 35. I-56126, Pisa, Italy,* [‡]*Dipartimento di Chimica Strutturale e Stereochimica Inorganica, Università di Milano, Via Venezian 21, I-20133 Milano, Italy, and* [§]*Dipartimento di Chimica, Università di Siena, Via A. Moro, I-53100 Siena, Italy*

Received July 22, 2009

The CuI catalyzed dehydro-halogenation of 1′,1‴-diethynylbiferrocene and $\{Pt_3\}Cl$ [$\{Pt_3\} = Pt_3(\mu\text{-}PBu^t_2)_3(CO)_2$] (1:2 molar ratio) in diethylamine gives in high yields the bicluster derivative $[\{Pt_3\}CC\text{-}(\eta^5\text{-}C_5H_4)Fe(\eta^5\text{-}C_5H_4)]_2$, **3**, in which two platinum triangles are connected by a diethynylbiferrocene spacer. In the structure of **3**, confirmed by a diffractometric study, the two $\{Pt_3\}$ fragments lie, perfectly eclipsed, on the same side of the biferrocenyl moiety; this folded structure is also preferred in solution, as suggested by NMR Diffusion Ordered Spectroscopy (DOSY) and 1D Rotating-frame Overhauser Enhancement (ROE) measurements. Compound **3** exhibits a rich redox behavior, with a crowded sequence of six one-electron oxidation processes, the electrode potentials of which have been evaluated by digital simulations. On the basis of a spectroelectrochemical study, the first two oxidations are assigned to the iron centers of the diferrocenyl unit and the subsequent four electrons are removed from the $\{Pt_3\}$ units.

Introduction

Soluble macromolecular assemblies containing transition metals are attracting considerable interest for their potential applications in nanomachine construction and molecular electronics.[1] An important class of such derivatives, very actively investigated, are molecular wires containing *mononuclear* metal fragments located at the extremes of, attached to, or directly embedded into, the main chain.[2] Analogous derivatives with metal−metal bonded *dinuclear* or *linear polynuclear* building blocks, by far less numerous, display rich electrochemical profiles and intrachain delocalization or interesting luminescence properties.[3] Beautiful 1-, 2-, or 3-D ordered structures have also been constructed using transition metal *molecular clusters* as structural units, connected by metal−metal bonds with transition or post-transition metals or by LL or $M(LL)_n$ units where LL is a bifunctional ligand.[4] The great majority of these assemblies, however, survive only in the solid state, being quite often either completely insoluble or easily depolymerized by the solvent. Soluble polymers with cluster units separated by strongly bound organic or organometallic spacers are rare, especially those with clusters inserted into the main macromolecular backbone.[5] Electron communication through the metal-spacer junction depends on the *relative* energy and symmetry of the molecular orbitals (MOs) of both partners, and the selection of suitable spacers

*To whom correspondence should be addressed. E-mail: leoni@dcci.unipi.it. Phone: +39 (0)50 2219217. Fax: +39 (0)50 2219217.

(1) (a) *Intelligent Materials*; M. Shahinpoor, M., H.-J. Schneider, H.-J., Eds.; RSC Publishing: Cambridge, 2008. (b) Balzani, V.; Credi, A.; Venturi, A. *Molecular Devices and Machines*; Wiley-VCH: Weinheim, 2003. (c) Wöhrle, D.; Pomogailo, A. D. *Metal Complexes and Metals in Macromolecules*; Wiley-VCH: Weinheim, 2003.

(2) (a) Manners, I. *Synthetic Metal-Containing Polymers*; Wiley-VCH: Weinheim, 2004.(b) Williams, K. A.; Boydston, A. J.; Bielawski, C. W. *Chem. Soc. Rev.* **2007**, *36*, 729–744. (c) Friese, V. A.; Kurth, D. G. *Coord. Chem. Rev.* **2008**, *252*, 199–211. (d) Wong, W. Y.; Ho, C.-L. *Coord. Chem. Rev.* **2006**, *250*, 2627–2690. (e) Zheng, Q.; Bohling, J. C.; Peters, T. B.; Frisch, A. C.; Hampel, F.; Gladysz, J. A. *Chem.—Eur. J.* **2006**, *12*, 6486–6505.

(3) (a) Tanase, T. *Bull. Chem. Soc. Jpn.* **2002**, *75*, 1407–1422. (b) Bérubé, J. F.; Gagnon, K.; D. Fortin, D.; Decken, A.; Harvey, P. D. *Inorg. Chem.* **2006**, *45*, 2812–2823. (c) Ren, T. *Organometallics* **2005**, *24*, 4854–4870. (d) Wang, C.-C.; Yang, C.-H.; Tseng, S.-M.; Lin, S.-Y.; Wu, T.-Y.; Fuh, M. R.; Lee, G.-H.; Wong, K.-T.; Chen, R.-T.; Cheng, Y.-M.; Chou, P.-T. *Inorg. Chem.* **2004**, *43*, 4781–4783. (e) Xue, W.-M.; Kühn, F. E.; Herdtweck, E.; Li, Q. *Eur. J. Inorg. Chem.* **2001**, 213–221. (f) Zhang, T.; Drouin, M.; Harvey, P. D. *Inorg. Chem.* **1999**, *38*, 957–963.

(4) (a) Selby, H. D.; Roland, B. K.; Zheng, Z. *Acc. Chem. Res.* **2003**, *36*, 933–944. (b) Mironov, Y. V.; Fedorov, V. E.; Bang, H.; Kim, S. J. *Eur. J. Inorg. Chem.* **2006**, 553–557. (c) Femoni, C.; Kaswalder, F.; Iapalucci, M. C.; Longoni, G.; Zacchini, S. *Chem. Commun.* **2006**, 2135–2137. (d) Zhang, J.; Lachgar, A. *J. Am. Chem. Soc.* **2007**, *129*, 250–251. (e) Jin, S.; DiSalvo, F. J. *Chem. Mater.* **2002**, *14*, 3448–3457. (f) Nakajima, T.; Ishiguro, A.; Wakatsuki, Y. *Angew. Chem., Int. Ed.* **2001**, *40*, 1066–1068. (g) Femoni, C.; Kaswalder, F.; Iapalucci, M. C.; Longoni, G.; Zacchini, S. *Eur. J. Inorg. Chem.* **2007**, 1483–1486.

(5) (a) Bradford, A. M.; Kristof, E.; Rashidi, M.; Yang, D.-S.; Payne, N. C.; Puddephatt, R. J. *Inorg. Chem.* **1994**, *33*, 2355–2363. (b) Johnson, B. F. G.; Sanderson, K. M.; Shephard, D. S.; Ozkaya, D.; Zhou, W.; Ahmed, H.; Thomas, M. D. R.; Gladdenc, L.; Mantle, M. *Chem. Commun.* **2000**, 1317–1318. (c) Wang, F.; Lai, Y.-H.; Han, M. Y. *Org. Lett.* **2003**, *5*, 4791–4794. (d) Randles, M. D.; Lucas, N. T.; Cifuentes, M. P.; Humphrey, M. G.; Smith, M. K.; Willis, A. C.; Samoc, M. *Macromolecules* **2007**, *40*, 7807–7818.

Published on Web 03/19/2010

Chart 1

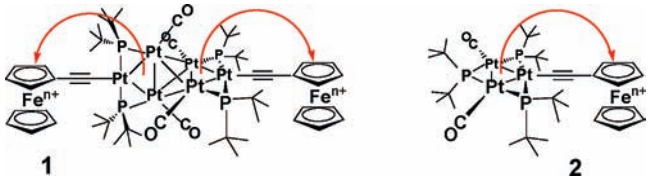

Scheme 1. Synthesis of the Bicluster Derivative **3**

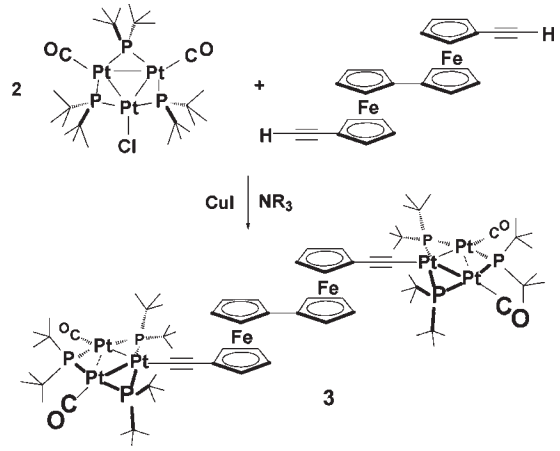

for a given cluster unit, crucial to impart the desired degree of charge transfer and the planned properties to the final materials, have still to be made empirically.

We have recently shown that sterically hindered hexanuclear and trinuclear platinum clusters are suitable precursors for ordered (linear[6a,b] or dendrimeric)[6c] "polycluster" materials and filmable polymers with alkynyl spacers.[6b] To investigate the charge transfer processes along these cluster units and ethynyl spacers we have already prepared the ferrocenyl derivatives $[Pt_6(\mu\text{-}PBu^t_2)_4(CO)_4(CC\text{-}Fc)_2]$, (**1**), and $[Pt_3(\mu\text{-}PBu^t_2)_3(CO)_2(CC\text{-}Fc)]$, (**2**), [Fc = $(\eta^5\text{-}C_5H_5)(\eta^5\text{-}C_5H_4)$Fe] (Chart 1, $n = 0$).[7a,b]

Electrochemical and spectroelectrochemical studies have shown the appearance of a photoelectrochemically triggered electron transfer from the $\{Pt_x\}$ core to the peripheral oxidized Fc subunits ($\mathbf{1}^{2+}$, $\mathbf{2}^{+}$, Chart 1, $n = 1$).[7a,b] These results, and the well-known complete electron delocalization within the biferrocenyl fragment,[8a] suggested that cluster-to-cluster electron transfer should have been observed in structure **3** (Scheme 1), where two triangular $Pt_3(\mu\text{-}PBu^t_2)_3(CO)_2$ (hereafter $\{Pt_3\}$) units are connected by a 1′,1‴-diethynylbiferrocene spacer.

Herein we describe the synthesis of the molecular wire **3** and its solid state structure, together with PGSE and NOE NMR studies which show that in solution compound **3** has a dicluster molecular pincer structure similar to the one observed in the solid state. Electrochemical and UV−vis−NIR spectroelectrochemical studies are complementary to assign the order in which the different redox centers are oxidized.

Results and Discussion

Complex **3** was prepared in high yield (90%) by the CuI catalyzed dehydrohalogenation of 1′,1‴-diethynylbiferrocene and the trinuclear halide $\{Pt_3\}Cl$ (1:2 molar ratio) in diethylamine solution; microanalytical and spectroscopic data (see Experimental Section) were fully consistent with the structure given in Scheme 1, which was then confirmed by a diffractometric study; single crystals of **3** were grown by slow evaporation of a CH_2Cl_2 solution. An Oak Ridge Thermal Ellipsoid Plot (ORTEP) view of the structure of **3** is shown in Figure 1.

The two cluster units in **3** maintain the usual features observed in related structures,[9] with the bulky *t*-butyl substituents hindering the central nearly planar $Pt_3(\mu\text{-}P_3)$ core; moreover, the two similar $\{Pt_3\}CCFc'$ (Fc′ = $(\eta^5\text{-}C_5H_4)_2Fe$) halves exhibit geometric parameters *similar* to those found in the structure of the closely related "monomer" **2**.[7b] The separations between the CO-bonded platinum centers are quite different (Pt2···Pt3 = 3.3621(4) and Pt5···Pt6 = 3.2615(4) Å) and comparable to the corresponding ones in the two independent molecules in the unit cell of complex **2**: 3.209(2) and 3.281(2) Å. We note that to the short Pt···Pt separation in **3** corresponds a significant lengthening of the Pt4−Pt(5,6) bonds (2.8350(4) and 2.8435(4) Å, respectively) compared to the Pt1−Pt(2,3) bonds, at 2.7967(4) and 2.7980(4) Å, and a closing of the Pt5−P5−P6 bond angle (89.72(3) vs 93.24(7)°) for the Pt2−P2−Pt3 angle. A similar soft potential for the deformation of the Pt···Pt interactions has been previously observed in the dendrimer $[(\{Pt_3\}CC)_2\text{-}C_6H_3\text{−}CC]_2[Pt_6(\mu\text{-}PBu^t_2)_4(CO)_4]$[6c] built from four chemically equivalent $\{Pt_3\}$ units where the longer and shorter Pt···Pt separations span the wide range: 3.066−3.380 and 2.785−2.914 Å, respectively. This effect has also been observed in other $Pt_3(\mu\text{-}PR_2)_3(L)_2X$ derivatives with σ-donor X ligands.[10] The planes containing the C_5H_4- rings are nearly coplanar with the adjacent Pt_3 planes (dihedral angles ca. 12° and 16°, respectively), suggesting π conjugation with the cluster moiety. Finally, it is worth noticing that the two $\{Pt_3\}$ fragments lie on the same side of the biferrocenyl moiety (*cisoidal* disposition) and, indeed, are perfectly eclipsed, although this forces one ferrocenyl unit to be nearly eclipsed and the other to have an anticlinal staggered conformation (Figure 1).

The stereochemical features of complex **3** in solution were investigated by NMR DOSY (Diffusion Ordered SpectroscopY)[11] and 1D ROE (Rotating-frame Overhauser Enhancement) techniques, which respectively enabled us to measure translational diffusion coefficients (D, $m^2\ s^{-1}$) and to detect through-space dipolar interactions.

(6) (a) Leoni, P.; Marchetti, F.; Marchetti, L.; Pasquali, M. *Chem. Commun.* **2003**, 2372–2373. (b) Leoni, P.; Marchetti, L.; Mohapatra, S. K.; Ruggeri, G.; Ricci, L. *Organometallics* **2006**, *25*, 4226–4230. (c) Albinati, A.; Leoni, P.; Marchetti, L.; Rizzato, S. *Angew. Chem., Int. Ed.* **2003**, *42*, 5990–5993.

(7) (a) Albinati, A.; Fabrizi de Biani, F.; Leoni, P.; Marchetti, L.; Pasquali, M.; Rizzato, S.; Zanello, P. *Angew. Chem., Int. Ed.* **2005**, *44*, 5701–5705. (b) Fabrizi de Biani, F.; Manca, G.; Marchetti, L.; Leoni, P.; Bruzzone, S.; Guidotti, C.; Zanello, P.; Atrei, A.; Albinati, A.; Rizzato, S. *Inorg. Chem.* **2009**, *48*, 10126.

(8) Colbert, M. C. B.; Hodgson, D.; Lewis, J.; Raithby, P. R.; Long, N. J. *Polyhedron* **1995**, *14*, 2759–2766.

(9) Cavazza, C.; Fabrizi de Biani, F.; Funaioli, T.; Leoni, P.; Marchetti, F.; Marchetti, L.; Zanello, P. *Inorg. Chem.* **2009**, *48*, 1385–1397.

(10) Bender, R.; Braunstein, P.; Dedieu, A.; Ellis, P. D.; Huggins, B.; Harvey, P. D.; Sappa, E.; Tiripicchio, A. *Inorg. Chem.* **1996**, *35*, 1223–1234.

(11) (a) Johnson, C. S., Jr. *Prog. Nucl. Magn. Reson. Spectrosc.* **1999**, *34*, 203–256. (b) Morris, G. A. Diffusion-ordered spectroscopy (DOSY). In *Encyclopedia of Nuclear Magnetic Resonance*; Grant, D. M., Harris, R. K., Eds.; John Wiley: Chichester, 2002; Vol. *9*, pp 35−44.(c) Macchioni, A.; Ciancaleoni, G.; Zuccaccia, C.; Zuccaccia, D. *Chem. Soc. Rev.* **2008**, *37*, 479–489.

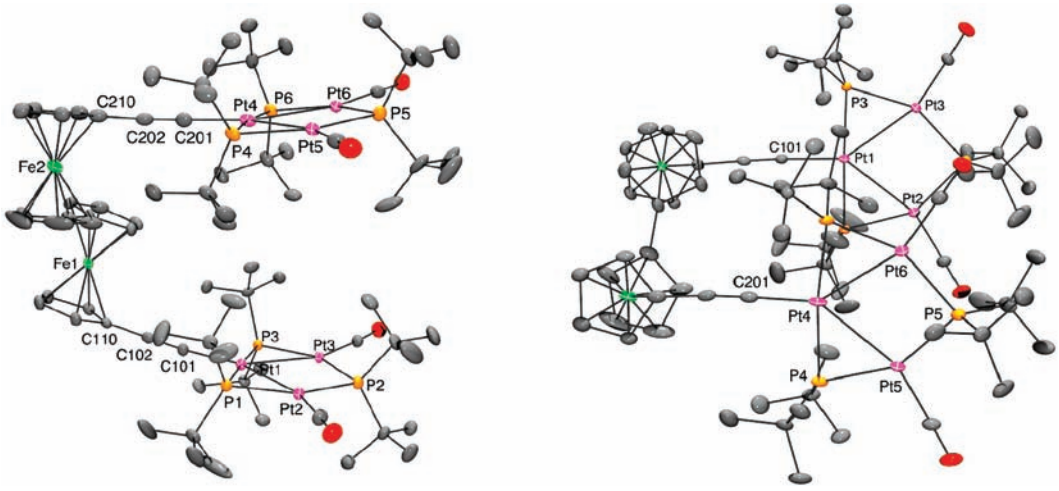

Figure 1. ORTEP views of the structure of **3** showing the atom numbering scheme. Thermal ellipsoids drawn at 50% probability. Selected bond lengths [Å] and angles [deg]: Pt1−Pt2 2.7967(4), Pt1−Pt3 2.7980(4), Pt2−Pt3 3.3621(4), Pt4−Pt5 2.8350(4), Pt4−Pt6 2.8435(4), Pt5−Pt6 3.2615(4), Pt−C101 1.970(7), Pt−C201 1.968(9), C119−C219 1.46(1), C≡C 1.21(1)*, C−O 1.130(7)*, Fe−C 2.05(1)*, Pt1−Pt2−Pt3 53.080(8), Pt2−Pt3−Pt4 53.046(8), Pt4−Pt5−Pt6 55.067(8), Pt5−Pt6−Pt4 54.823(9). (* av. values).

Table 1. Diffusion Coefficients (D, 600 MHz, 25 °C) of **3**, Calculated Perrin Factor (f_p), and Axial Ratio (P) for a Prolate and an Oblate Model

	C_6D_6	CD_2Cl_2
D ($\times 10^{10}$ m^2 s^{-1})	4.1	5.9
f_p	1.019	1.052
P (prolate)[a]	0.632 (8.7)	0.471 (11.7)
P (oblate)[a]	1.592 (8.8)	2.165 (11.9)

[a] The calculated major semiaxes (Å) are reported in parentheses; obtained by prefixing at 5.5 Å the minor semiaxis (from crystallographic data).

Diffusion coefficients of complex **3** were measured in C_6D_6 and CD_2Cl_2 (Table 1), by using tetramethylsilane, $SiMe_4$, a spherical molecule with negligible tendency to associate in solution, as an internal standard for viscosity.[12] As detailed in the Supporting Information, the shape of the molecule was approximated to an ellipsoid of revolution generated by an ellipse with semiaxes a and b and revolving about its major or minor axis for, respectively, prolate or oblate ellipsoids. According to this model a correction factor f_p (Perrin factor)[13] was extracted from experimental diffusion coefficients to evaluate axial ratios P for oblate/prolate ellipsoids (Table 1).

In C_6D_6, the calculated major semiaxes for the oblate model of **3** (Table 1) were in optimal agreement with those observed in the solid-state conformation **A** (Figure 2). On the other hand, for the prolate model a major semiaxis of 8.7 Å was calculated (Table 1), too short for any of the prolate structures **B**−**E** (Figure 2), which, therefore, should not be significantly populated in solution.

In CD_2Cl_2, the calculated semiaxes for both the prolate and the oblate models (Table 1) suggest the coexistence of **A** with significant amounts of the partially rotated prolate conformers **D** and/or **E** (Figure 2). 1D ROE measurements (see Supporting Information) in CD_2Cl_2 confirmed these assumptions (no valid information can be obtained from spectra in C_6D_6, in which two aromatic resonances are completely superimposed), ruling out the presence of significant amounts of conformer **B**, and allowed us to exclude also a significant contribution of conformer **E**.

Thus, on the basis of diffusion and ROE data, it can be concluded that complex **3** is mainly present in CD_2Cl_2 solution as a mixture of conformers very close to the solid-state structure **A** and to its partially rotated **D** stereoisomer. All attempts to obtain decoalescence of NMR signals by low temperature (down to −70 °C) experiments were unsuccessful. The prevalence of folded conformers of **3** both in the solid state and in solution can reasonably be ascribed to hydrophobic interactions between the *t*-butyl layers of the adjacent cluster units. This stacking propensity could be exploited in the future for the synthesis of cluster-containing porous materials.

Electrochemistry. As a general feature, [{Pt_3}X] clusters exhibit two one-electron oxidations.[9] Moreover, as expected, compound **2** undergoes a further, ferrocenyl-centered, one-electron oxidation.[7b] Because of the presence of multiple redox active sites, and for the reasons detailed in the Introduction, it was predicted that compound **3** should exhibit a rich redox behavior. In fact, as shown in Figure 3 (full line), cyclic voltammetry reveals a crowded sequence of oxidation processes in the range 0−1 V, in which the low separation of the different processes makes the direct evaluation of redox potentials difficult, even using pulsed voltammetric techniques (dashed lines). Therefore, the pertinent values have been extracted by digital simulations by using the DigiSim 3.03 program.[14]

To obtain a consistent set of parameters, the cyclic voltammograms at 0.02 and 0.5 V s^{-1} have been simulated at once. As shown in Figure 4, the presence of the inflection at about 0.5 V makes plausible to propose a mechanism involving a sequence of six redox reactions. The adjustable parameters in the simulation procedure are standard potentials, heterogeneous rate constants, and diffusion coefficients. Under the assumption of

(12) Cabrita, E. J.; Berger, S. *Magn. Reson. Chem.* **2001**, *39*, S142–S148.
(13) (a) Cantor, C. R.; Schimmel, P. R. *Biophysical chemistry, Part II: Techniques for the study of biological structure and function*; Freeman, W. H.: New York, 1980; pp 530−590.(b) Durchschlag, H.; Zipper, P. *J. Appl. Crystallogr.* **1997**, *30*, 1112–1124.

(14) Rudolph, M.; Feldberg, S. W. *DigiSim*, version 3.03; Bioanalytical Systems: West Lafayette, IN, 2009.

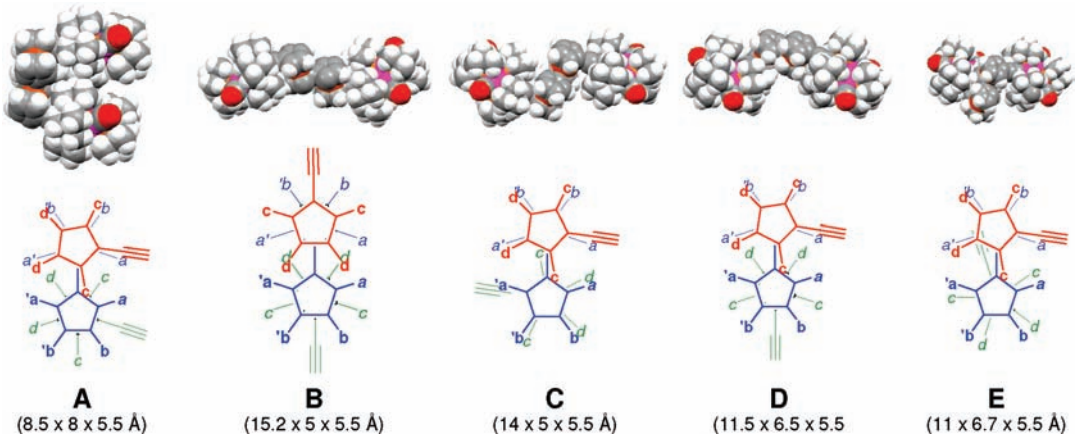

Figure 2. Stereoisomers of the bicluster derivative **3**. Top: space-filling models; bottom: wireframe models (clusters omitted for clarity; blue: fulvalene; red and green: cluster substituted rings). The length of the semiaxes for conformers **A**−**E**, reported in parentheses, were estimated by the space-filling models. Structure **A** is identical to the one observed in the solid-state, conformers **B**−**E** were obtained from the latter by rotations around the main axis passing through Fe and the center of the cyclopentadienyl rings of one or both the ferrocene units. During rotations all other bond lengths and angles were kept constant.

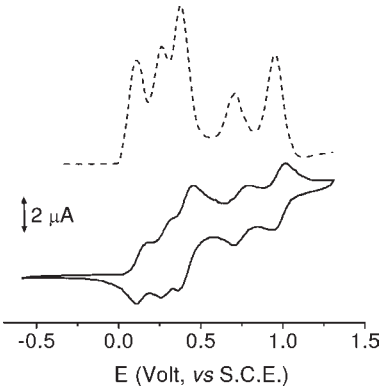

Figure 3. Cyclic (full line) and differential pulse (dashed line) voltammograms of 1.0 mM of **3**. Scan rates 0.02: V s^{-1} in 0.2 M $[NBu_4]PF_6/CH_2Cl_2$.

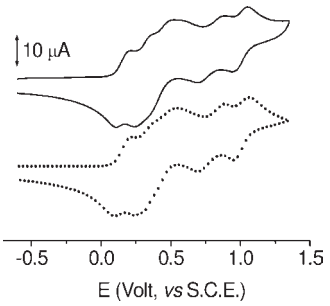

Figure 4. Experimental (full line) and simulated (dotted line) cyclic voltammograms of 1.0 mM of **3** at scan rates of 0.5 V s^{-1} in 0.2 M $[NBu_4]PF_6/CH_2Cl_2$. The simulation parameters employed are reported in Table 2.

simple electrochemical electron transfer processes, the symmetry factors have been kept fixed at 0.5.[15] Even if the diffusion coefficient is expected to vary for differently charged species, initially they have all been kept fixed at 6.0×10^{-10} m^2 s^{-1}. Once the remaining parameters had been optimized, the diffusion coefficients have been partially relaxed, but constrained to have the same value. The final value is 5.5×10^{-10} m^2 s^{-1}, which does not diverge significantly from the initial one, and is in good agreement with the value obtained by NMR. The simulated redox potentials are reported in Table 2 together with the experimental redox potentials of some related compounds.

Since for most of the scan rates employed the k_s values are around 10^{-2} cm s^{-1}, the electrode processes may be considered as quasireversible.[18] By keeping in mind that **2** undergoes three oxidations, the key point here is the presence of six oxidations for **3**. This could imply not only that the electron delocalization within the biferrocenyl fragment is maintained but also that the two $\{Pt_3\}$ moieties are able to interact through the diethynylbiferrocene bridge.

By looking at Table 2, it is evident that the attribution of each oxidation to the different redox centers is not straightforward. In fact, neither the absolute potential values nor their relative positions are a reliable guide in the assignment of the redox processes. As a general trend, owing to coordination, both the biferrocene oxidations are cathodically shifted with respect to free 1′,1‴-diethynylbiferrocene,[8] but this effect is not easily quantifiable and affects the first and the second redox processes to a different extent, so that the $\Delta E^{\circ\prime}_{Fe-Fe}$ separation, which may be a probe of electronic communication between the two iron centers, can increase or decrease.

In the case of **2**, a detailed experimental and theoretical study confirmed that the first oxidation is centered on ethynylferrocene, while the second and third processes are centered on the $\{Pt_3\}$ moiety.[7b]

On this basis, we confidently assign the first oxidation of **3** to one ferrocenyl and, on the basis of the subsequent discussion, the second oxidation to the other ferrocenyl subunit. This means that the successive four oxidations arise from electron removals from the $\{Pt_3\}$ units. Indeed, even if different combinations of oxidation processes are possible, experimental evidence support this attribution, in that, not only the heterogeneous rate constants k_s for the first two oxidations are substantially similar, but, as it will be discussed in the following section, also the spectroelectrochemical behavior appears consistent with the assignment.

(15) (a) Marcus, R. A. *J. Chem. Phys.* **1965**, *43*, 679–701. (b) Hush, N. S. *Trans. Faraday Soc.* **1961**, *57*, 557–580.

Table 2. Simulated Redox Potentials of **3** and Experimental Redox Potentials of Some Related Compounds (Volt, vs S.C.E.), in CH_2Cl_2 Solution

	$E^{\circ\prime}$						$\Delta E^{\circ\prime}$(Fe−Fe)	ref.
3[a]	+0.14	+0.28	+0.40	+0.46	+0.77	+0.98	0.14	this work
$(HCCFc)_2$	+0.47[b]	+0.79[b]					0.32	8
$(HCCFc)_2\{Mn\}_2$[c,d]	+0.19	+0.44					0.25	8
$(HCCFc)_2\{Ru\}_2$[c,e]	+0.02	+0.18					0.16	8
$(HCCFc)_2\{Pt'Ph\}_2$[c,f]	+0.19	+0.57					0.38	16
$(HCCFc)_2\{Pt''Ph\}_2$[c,g]	+0.15	+0.53					0.38	16
$[(HCCFc)_2\{Pt''\}_2]_n$[c,g]	+0.30	+0.57					0.27	16
2	+0.18		+0.37	+0.73				7b
HCCFc	+0.57							17

[a] The k_s[b] ($\times 10^{-3}$) values for the six redox processes are 6.6; 6.0; 4.7; 1.2; 2.0; 5.0 cm s^{-1}. [b] Loosely converted to S.C.E. [c] Only the redox processes relating to diethynylbiferrocene are indicated. [d] {Mn} = $Mn(CO)_3Ph_2PCH_2PPh_2$. [e] {Ru} = $Mn(Ph_2PCH_2PPh_2)_2Cl$. [f] {Pt′} = $Pt(PEt_3)_2$. [g] {Pt″} = $Pt(PBu^n_3)_2$.

As observed in other cases, in **3** there is a significant destabilization of the Fe^{II} centers toward oxidation; in fact, the first and second ferrocene-centered oxidations take place at potentials 330 and 510 mV less positive, respectively, than in free 1′,1‴-diethynylbiferrocene.[8] It can also be seen that going from 1′,1‴-diethynylbiferrocene to **3**, the separation $\Delta E^{\circ\prime}_{Fe-Fe}$ decreases. This may be due to the fact that the replacement of the ethynyl protons by platinum clusters allows the delocalization of the positive charge on the $\{Pt_3\}$ units, so attenuating the Coulombic interaction between the iron centers, and/or to the fact that the electronic communication caused by the resonance is lowered. As a result, the stability of the $Fe^{II}Fe^{III}$ mixed-valence species is also lowered with respect to disproportionation. As discussed previously, the two sequential oxidations at +0.40 and +0.46 V should be ascribed to the first electron removal from each $\{Pt_3\}$ unit. ΔE is small, but not negligible and, in fact, because of the complexity of the system under study and of the weakness, if any, of the electronic interaction between the two $\{Pt_3\}$ units through the diethynylferrocene bridge, it has not been possible to draw any decisive conclusion on the degree of charge delocalization between them. This matter will be the subject of another paper in which we plan to compare the effect of a few different bridging ligands in a series of $\{Pt_3\}$-L_B-$\{Pt_3\}$ recently characterized in our laboratory (L_B = butadiyndiyl, 1,4-bis(ethynyl)benzene, 2,5-bis(ethynyl)thiophene, 9,10-bis(ethynyl)anthracene). Finally, the couple of oxidations at +0.77 and +0.98 V should be ascribed to the separate second electron removal from the two $\{Pt_3\}$ units. The fact that the pertinent $\Delta E^{\circ\prime}$ ($\Delta E^{\circ\prime}$ = 210 mV) is higher than that of the two first one electron removals ($\Delta E^{\circ\prime}$ = 60 mV) may be a prelude to the stepwise increase of the electronic communication between the two oxidized $\{Pt_3\}$ units. From a qualitative viewpoint this could well be possible in view of (i) the expected contraction of the Pt_3 triangle upon oxidation that may alter significantly either the energy of the platinum orbitals and the extent to which they overlap with the diethynylbiferrocenium orbitals (thus modifying the electronic communication), (ii) the electrostatic effects due to the increasing charge of the whole system.

Controlled potential coulometry of **3** (E_w = +0.25 V) proceeds very slowly. Cyclic voltammograms recorded after the exhaustive one-electron oxidation show that cation $\mathbf{3}^+$ decomposes rapidly as indicated by the appearance of a new redox profile with two reversible oxidations at +0.56 and +0.90 V. It may then be assumed that the process is accompanied by the release of diethynylbiferrocene, in that the redox potentials reported in ref 8 do not allow a precise conversion to S.C.E.

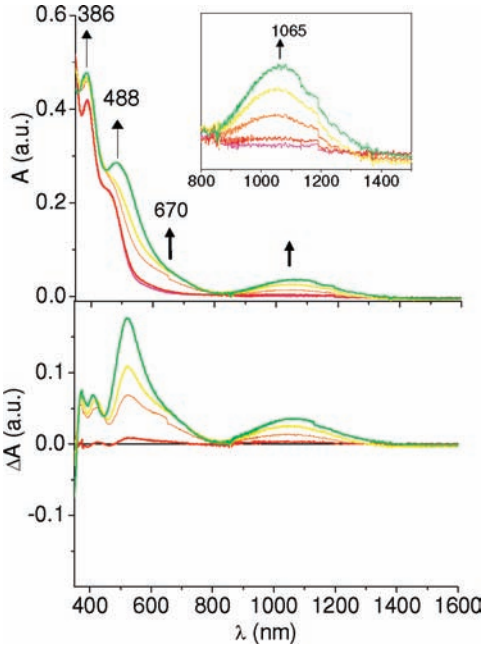

Figure 5. UV−vis−NIR (top) and difference spectra (bottom) recorded in a OTTLE cell upon stepwise two electrons removal from **3** in CH_2Cl_2 solution. $[NBu_4][PF_6]$ (0.2 mol dm^{-3}) supporting electrolyte.

Spectroelectrochemistry. The UV−vis spectral changes accompanying the stepwise oxidation of **3** have been followed in situ using an OTTLE cell. In spite of the lability of the electrogenerated species in the long times of macroelectrolysis, the spectroelectrochemical measurements were useful to determine the nature of the mixed-valent species electrogenerated at the different anodic process. Since the chemical complications following the electron removals would have made the measurement of molar absorptions rather doubtful, the spectral absorptions are expressed in arbitrary units.

As illustrated in Figure 5, the first and second electron removals are accompanied by the occurrence of two main features: the appearance of a peak at 488 nm,

(16) Long, N. J.; Martin, A. J.; Vilar, R.; White, A. J. P.; Williams, D. J.; Younus, M. *Organometallics* **1999**, *18*, 4261–4269.
(17) Fink, H.; Long, N. J.; Martin, A. J.; Opromolla, G.; White, A. J. P.; Williams, D. J.; Zanello, P. *Organometallics* **1997**, *16*, 2646–2650.
(18) Zanello, P. *Inorganic electrochemistry. Theory, practice and application*; RSC: Oxford, 2003.

superimposed to the original peak at 464 nm, and the growth of a weak and broadband in the NIR region at 1065 nm. This feature is highly reminiscent of what has been observed upon stepwise one-electron oxidation of complex **2**, in which the corresponding bands were located at ~530 and 1135 nm, respectively.[7b]

In that case, a detailed TDDFT study allowed to ascribe them to Metal-to-Metal Charge Transfers (MMCT) from the Pt_3 cluster to the ferrocenium subunit, and it seems reasonable to make a similar assignment for **3**.[19] A shoulder at ~670 nm is also detectable, and may confidently be assigned to the typical blue-to-green ferrocenium absorption.[20]

The overall behavior fits well with the assignment of the redox processes proposed previously: in fact, the continuous growth of *both* the bands at 488 and 1065 nm ($\{Pt_3\}\rightarrow Fe^{III}$ MMCT) and of that at 670 nm (Fe^{III} d→d) agrees with the progressive formation of one and two Fe^{III} centers in the molecule upon the first and second electron removal and, at the same time, rules out the assignment of the NIR band as merely caused by the (expected) Inter-Valence-Charge-Transfer (IVCT) absorption of the one-electron oxidized biferrocenium bridge. Anyway, the $Fe^{II}\rightarrow Fe^{III}$ IVCT may be easily hidden by the broad NIR band.

Experimental Section

General Data. All manipulations involving air-sensitive materials were carried out by using standard Schlenk techniques under an atmosphere of N_2. Solvents were dried by conventional methods and distilled under nitrogen prior to use. $Pt_3(\mu\text{-}PBu^t_2)_3(CO)_2Cl$[6c] and 1′,1‴-diethynylbiferrocene[8] were prepared as previously described. IR spectra were recorded with a Perkin-Elmer Fourier transform IR 1725X spectrophotometer. NMR spectra were acquired using a Varian Gemini 200 BB spectrometer (200 MHz for ^1H NMR) at room temperature (about 293 K). The # symbol is used to label ^1H, ^{13}C, and ^{31}P peaks with ^{195}Pt satellites. DOSY and ROE measurements were performed on a spectrometer operating at 600 MHz for ^1H. The temperature was controlled to ±0.1 °C. ^1H chemical shifts are referenced to tetramethylsilane, $SiMe_4$, as internal standard. The 2D NMR spectra were obtained by using standard sequences. Proton gCOSY 2D spectra were recorded in the absolute mode acquiring 4 scans with a 5 s relaxation delay between acquisitions for each of 256 FIDs. Proton 1D ROE spectra were recorded using selective pulses generated by means of the Varian Pandora Software. The 1D ROE spectra were acquired with 128 scans in 32K data points with a 5 s relaxation delay and a mixing time of 0.6 s. The gradient HMBC (Heteronuclear Multiple Bond Correlation) experiments were optimized for a long-range $^1H-^{13}C$ coupling constant of 8 Hz. The spectra were acquired with 256 time increments, 32 scans per t_1 increment and a 3.5 ms delay period for suppression of one-bond correlation signals. No decoupling during acquisition was used. DOSY experiments were carried out by using a stimulated echo sequence with self-compensating gradient schemes and a spectral width of 5600 Hz. A value of 160 ms was used for Δ, 1.0 ms for δ, and *g* was varied in 30 steps (8 transients each) to obtain an approximately 90−95% decrease in the resonance intensity at the largest gradient amplitudes. The baselines of all arrayed spectra were corrected prior to processing the data. After data acquisition, each FID was apodized with 1.0 Hz line broadening and Fourier transformed. The data were processed with the DOSY macro (involving the determination of the resonance heights of all the signals above a pre-established threshold and the fitting of the decay curve for each resonance to a Gaussian function) to obtain pseudo two-dimensional spectra with NMR chemical shifts along one axis and calculated diffusion coefficients along the other.

Table 3. Experimental Data for the X-ray Diffraction Study of Compound **3**·(CH_2Cl_2)

formula	$C_{77}H_{126}Cl_2Fe_2O_4P_6Pt_6$
mol wt	2654.74
data coll. *T*, K	110 (2)
diffractometer	Bruker APEX II CCD
cryst syst	monoclinic
space group (no.)	$P2_1/n$ (14)
a, Å	16.2468(4)
b, Å	17.2413(5)
c, Å	32.2565(9)
β, deg	90.269(1)
V, Å^3	9035.5(4)
Z	4
$\rho_{(calcd)}$, g cm^{-3}	1.952
μ, cm^{-1}	97.70
radiation	Mo Kα (graphite monochrom., λ = 0.71073 Å)
θ range, deg	1.83 < θ < 26.05
no. data collected	82255
no. independent data	17756
no. obs. refctl. (n_o) [$\lvert F_o\rvert^2 > 2.0\sigma(\lvert F\rvert^2)$]	14943
no. of param. refined (n_v)	874
R_{int}[a]	0.0359
R (obsd reflns)[b]	0.0361
R^2_w (obsd reflns)[c]	0.0919
GOF[d]	1.042

[a] $R_{int} = \sum\lvert F_o^2 - \langle F_o^2\rangle\rvert/\sum F_o^2$. [b] $R = \sum(\lvert F_o - (1/k)\ F_c\rvert)/\sum\lvert F_o\rvert$. [c] $R^2_w = \{\sum[w(F_o^2 - (1/k)F_c^2)^2\ ]/\sum w\lvert F_o^2\rvert^2]\}^{1/2}$. [d] GOF = $[\sum_w(F_o^2 - (1/k)F_c^2)^2/(n_o - n_v)]^{1/2}$.

Preparation of 3. 1′,1‴-Diethynylbiferrocene (28.1 mg, 0.067 mmol) and CuI (0.255 mg, 1.34 μmol) were added to a brown diethylamine solution of $Pt_3(\mu\text{-}PBu^t_2)_3(CO)_2Cl$ (150 mg, 0.135 mmol). After stirring for 24 h at room temperature, the solvent was evaporated, and the brown residue was extracted with toluene to give, after chromatography (silica gel, eluent toluene/*n*-hexane 2:1) 155 mg of **3** (90%) as a microcrystalline solid. Elemental Analysis (%) calcd for $C_{76}H_{128}Fe_2O_4P_6Pt_6$: C, 35.5, H, 5.01; Found: C, 35.4, H, 4.96. $^{31}P\{^1H\}$ NMR δ = 168.6# (d, $^2J_{PP}$ = 129 Hz, 2 P). 92.8# ppm (t, $^2J_{PP}$ = 129 Hz, 1 P); ^1H NMR (C_6D_6) δ = 4.41 (s, 1 H, Cp), 4.22 (s, 2 H, Cp), 3.97 (s, 1 H, Cp), 1.45 (vt, $^3J_{HP} + {}^5J_{HP}$ = 5.8 Hz, 18 H, CH_3), 1.35 ppm (d, $^3J_{HP}$ = 14.7 Hz, 9 H, CH_3). $^{13}C\{^1H\}$ NMR δ = 175.5# (s, CO), 118.4 (s, Pt−C≡*C*), 85.6 (s, Pt−*C*≡C), 69.4, 71.2 (s, i-C, Cp), 68.1, 69.6, 70.8, 71.6 (s, CH, Cp), 39.2 (s, *C*CH_3), 33.9 ppm (s, CH_3). $^{195}Pt\{^1H\}$ NMR δ = −6125 (t, $^1J_{PtP}$ = 2151 Hz, 1Pt), −5691 ppm (t, $^1J_{PtP}$ = 1887 Hz, 2Pt). IR (CH_2Cl_2) = 2103 ($\nu_{C\equiv C}$), 2019 ($\nu_{C\equiv O}$) cm^{-1}.

Electrochemistry and Spectroelectrochemistry. Anhydrous 99.9%, HPLC grade dichloromethane for electrochemistry was purchased from Aldrich. The supporting electrolyte used was electrochemical grade $[NBu_4][PF_6]$ obtained from Fluka. Cyclic voltammetry was performed in a three-electrode cell having a platinum working electrode surrounded by a platinum-spiral counter electrode and the aqueous saturated calomel reference electrode (SCE) mounted with a Luggin capillary. Either a BAS 100A or a BAS 100W electrochemical analyzer

(19) (a) An earlier report[19b] by Robinson et al. on a 17-electron $[FeC_2R]^+$ ferricenium ion showed a NIR band at similar energy that was assigned to an LMCT transition, i.e., charge transfer from the donor R to the acceptor $[Fc]^+$, which could be considered as analogous to our assignment of MMCT where the Pt unit is the donor linked by C_2 to the acceptor $[Fc]^+$.(b) Flood, A. H.; McAdam, C. J.; Gordon, K. C.; Kjaergaard, H. G.; Manning, A. M.; Robinson, B. H.; Simpson, J. *Polyhedron* **2007**, *26*, 448.

(20) Hendrickson, D. N.; Sohn, Y. S.; Duggan, D. M.; Gray, H. B. *J. Chem. Phys.* **1973**, *58*, 4666.

was used as a polarizing unit. Controlled potential coulometry was performed in an H-shaped cell with anodic and cathodic compartments separated by a sintered-glass disk. The working macroelectrode was a platinum gauze; a mercury pool was used as the counter electrode. All reported potential values are referred to the saturated calomel electrode (SCE). Under the experimental conditions, the one-electron oxidation of ferrocene occurs at $E^{o\prime} = +0.39$ V. UV−vis spectroelectrochemical measurements were carried out using a Perkin-Elmer Lambda 900 UV−vis spectrophotometer and an optically transparent thin-layer electrode cell (OTTLE cell) equipped with a Pt-minigrid working electrode (32 wires/cm), Pt minigrid auxiliary electrode, Ag wire pseudoreference and CaF_2 windows.[21] During the microelectrolysis procedures, the electrode potential was controlled by an Amel potentiostat 2059 equipped with an Amel function generator 568. Nitrogen-saturated CH_2Cl_2 solutions of the compound under study were used with $[NBu_4][PF_6]$ (2.0×10^{-3} mol dm^{-3}) as supporting electrolyte. The in situ spectroelectrochemistry has been recorded by collecting spectra, in the spectral window from 220 to 3000 nm, during the stepwise oxidation of the compound obtained by continuously increasing the potential from 0 to 1.1 V at a scan rate of 250 μV s^{-1}.

Crystallography. An air stable, red crystal of $\mathbf{3}\cdot CH_2Cl_2$ (obtained by slow evaporation from a dichloromethane solution) was mounted on a Bruker APEX II CCD diffractometer and cooled, using a cold nitrogen stream, to 110(2) K for the data collection. The space group was determined from the systematic absences, while the cell constants were refined, at the end of the data collection, with the data reduction software SAINT.[22] The experimental conditions for the data collection, crystallographic and other relevant data are listed in Table 3 and in the Supporting Information.

The collected intensities were corrected for Lorentz and polarization factors[22] and empirically for absorption using the SADABS program.[23] The structure was solved by direct and Fourier methods and refined by full matrix least-squares,[24] minimizing the function $[\sum w(F_o^2 - (1/k)F_c^2)^2]$ and using anisotropic displacement parameters for all atoms, except the hydrogens. The Difference Fourier maps showed clearly the presence of a clathrated CH_2Cl_2 molecule that was included and refined anisotropically.

No extinction correction was deemed necessary. Upon convergence the final Fourier difference map showed no significant peaks. The contribution of the hydrogen atoms, in their calculated positions, was included in the refinement using a riding model ($B(H) = aB(C_{bonded})$(Å^2), where $a = 1.5$ for the hydrogen atoms of the methyl groups and $a = 1.3$ for the others). The scattering factors used, corrected for the real and imaginary parts of the anomalous dispersion, were taken from the literature.[25] All calculations were carried out by using the PC version of the programs: WINGX,[26] SHELX-97,[24] and ORTEP.[27]

Acknowledgment. This work was supported by Ministero dell'Istruzione, dell'Università e della Ricerca (MIUR), Programmi di Interesse Nazionale, 2006 and 2007.

Supporting Information Available: Tables of crystal data and bond lengths and angles for **3** (as a CIF file). ^{1}H NMR spectra and characterization of **3** in C_6D_6 and CD_2Cl_2. Diffusion coefficients treatment and 1D ROE spectra. This material is available free of charge via the Internet at http://pubs.acs.org.

(21) Krejčik, M.; Daněk, M.; Hartl, F. *J. Electroanal. Chem.* **1991**, *317*, 179.
(22) *BrukerAXS, SAINT, Integration Software*; Bruker Analytical X-ray Systems: Madison, WI, 1995.
(23) Sheldrick, G. M. *SADABS, Program for Absorption Correction*; University of Göttingen: Göttingen, Germany, 1996.
(24) Sheldrick, G. M. *Acta Crystallogr.* **2008**, *A64*, 112.
(25) *International Tables for X-ray Crystallography*; Wilson, A. J. C., Ed.; Kluwer Academic Publisher: Dordrecht, The Netherlands, 1992; Vol. *C*.
(26) Farrugia, L. J. *J. Appl. Crystallogr.* **1999**, *32*, 837.
(27) Farrugia, L . J. *J. Appl. Crystallogr.* **1997**, *30*, 565.